Visualizing cell-cell interactions between immune effector and tumor cells induced by antibodies using a proximity-dependent biosensor system

Yu Tang [1] and Yanguang Cao [1, 2 #]

[1]Division of Pharmacotherapy and Experimental Therapeutics, UNC Eshelman School of Pharmacy, University of North Carolina at Chapel Hill, Chapel Hill, North Carolina. 27599, United States.

[2]Lineberger Comprehensive Cancer Center, School of Medicine, University of North Carolina at Chapel Hill, Chapel Hill, NC 27599, United States.

[#] **To whom correspondence should be addressed:** Yanguang Cao, UNC Eshelman School of Pharmacy, UNC at Chapel Hill. Tel: (919) 966-4040, Email: yanguang@unc.edu

Abstract

Therapeutic antibodies can engage innate (NK) and adaptive (T) immune cells to eliminate pathogenic or malignant cells. Activated NK or T cells exert cytotoxic effects dependent upon direct cell-cell contact and subsequent formation of immunological synapses (IS) with target cells. Therefore, understanding antibody-mediated cell-cell interactions is crucial to optimizing antibody pharmacology and efficacy across all therapeutic areas. To date, most investigations around antibody-mediated cell-cell interactions have primarily focused on molecular-scale interactions. In this study, we developed a biosensor system to evaluate direct cell-cell contact and interactions and the formation of IS at the cell population level. In this biosensor system, two structural complementary luciferase units (SmBit and LgBit) were respectively expressed on immune effector and target cell membranes with optimized spacer lengths. Upon cell-cell contact, two subunits come together to form active NanoLuc, generating a luminescent signal for longitudinal monitoring. The selectivity of the system were optimized by adjusting the spacer lengths to assure the signal is from stable cell-cell interactions with minimal interference from nonspecific and transient intercellular contact. This system was then applied to longitudinally quantify cell-cell interactions between NK and target cells induced by an anti-CD20 antibody (rituximab) and between T and target cells induced by a bispecific (anti-CD3/CD19) T cell engaging antibody (blinatumomab) in a three-dimensional cell culture system. This biosensor system shows promise for monitoring cell-cell interactions in physiologically relevant environments and provides insights into the environmental factors that impede cell-cell interaction and antibody efficacy.

Introduction

Therapeutic antibodies can engage innate (NK) and adaptive (T) immune cells to eliminate pathogenic or malignant cells[1,2]. Immune cell activation and intercellular interaction between immune effector and target cells are key to many antibody-based therapeutic approaches, including but not limited to checkpoint blockade, circulating cytokine neutralization, bispecific T cell engagement, and virus neutralization[3-5]. Characterizing antibody-induced cell-cell interactions between immune effector and target cells is therefore crucial to understanding antibody pharmacodynamics (PD). The factors that impede effective intercellular interaction inform the mechanisms of immune evasion and treatment resistance and potential strategies for optimizing antibody therapeutics across all therapeutic areas.

Interactions between effector and target cells entail multiple cellular steps, such as the trafficking of effector cells to target cells, the slowing of motility upon recognition, and the establishment of intercellular adhesion. The functions of effector cells in finding and engaging target cells could be impaired in many pathological environments, such as tumor microenvironments[6]. Many environmental factors work jointly to develop a niche that can restrict effector cells infiltration, motility, adhesion, and effector functionality[7]. To date, the majority of investigations around antibody-mediated cell-cell interactions have focused on molecular-scale interactions[8]. The dynamics of cell-cell direct contact and interactions and the formation of immunological synapse (IS) at the cell population level are critical for critical for understanding these intercellular steps but remain inadequately characterized.

Stable adherence between immune effector and target cells is the first step for intercellular interaction and a critical step for the formation of IS. Here we constructed a proximity-based biosensor system to detect stable intercellular contact and interaction. Briefly, two structurally complementary luciferase subunits in the NanoBiT® system[9], Large_BiT and Small_BiT, upon transfection, were respectively displayed on the surfaces of immune effector and tumor cells. Upon cell-cell contact and interaction, the proximity between tumor and immune cells allows the binding of Large_BiT and Small_BiT, forming active luciferases that emit strong luminescence upon substrate stimulus[9]. The system was optimized by adjusting the spacer lengths to detect stable cell-cell contact and IS formation with high specificity and sensitivity (high signal-to-noise (S/N) ratios). The system was applied to detect NK-tumor cell interactions induced by an anti-CD20 antibody rituximab and T-tumor cell interactions induced by a bispecific T cell engaging antibody blinatumomab in a three-dimensional (3D) cell culture system. Our studies demonstrated this biosensor system's great potential in monitoring cell-cell interactions in pathophysiologically relevant conditions, and the system supports evaluation of environment and physiological factors that impede effective cell-cell interactions and antibody efficacy.

Materials and Methods

Plasmid Construction

The pDisplay vector was used as a eukaryotic expression vector. Briefly, the murine Ig k chain leader sequence and platelet-derived growth factor receptor transmembrane domain (PDGFR-TM) are located at the inserted gene's N-terminus or C-terminus, which direct and anchor the fusion protein to the cell membrane[10]. The HA and myc epitopes on both sides of the expressed recombinant proteins allow the detection of fusion peptides (Figure 1).

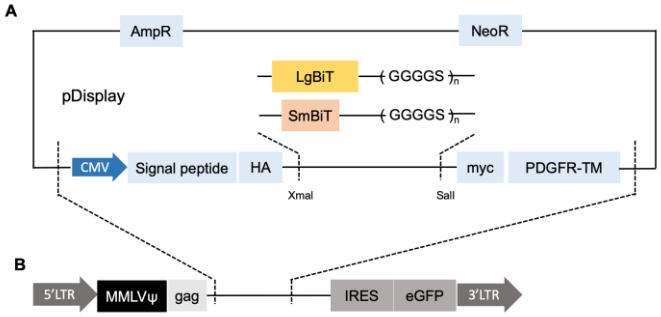

Figure 1: Construction of biosensor system plasmids. (A) LgBiT or SmBiT constructed in pDisplay vector. (B) The CMV-LgBiT-(GGGGS)n-PDGFR-TM gene was cloned into PBMN-I-eGFP.

The sequences of SmBiT and LgBiT were kindly provided by Promega. Spacers were added to the C terminus of LgBiT or SmBiT to yield different distances between split luciferases and cell membranes. The LgBiT-$(GGGGS)_n$ or SmBiT-$(GGGGS)_n$ sequences were inserted into the pDisplay plasmid at XmaI and SaLI restriction sites. The CMV-LgBiT-$(GGGGS)_n$-PDGFR-TM gene was cloned into PBMN-I-eGFP to produce recombinant retrovirus. PBMN-I-GFP was a gift from Garry Nolan (Addgene plasmid # 1736; http://n2t.net/addgene:1736; RRID:Addgene_1736)

Cell Culture and Transductions

HeLa cells were cultured in complete media: DMEM with 10% (vol/vol) FBS (Invitrogen), 100U/mL penicillin, and 100 mg/mL streptomycin (all from Gibco). Phoenix-AMPHO cells (ATCC® CRL-3212™) were cultured in RPMI 1640 medium supplemented with 10% (vol/vol) FBS (Invitrogen), 100U/mL penicillin, and 100 mg/mL streptomycin (all from Gibco). Human Natural Killer cell line (NK-CD16; no GFP, high affinity 176V; SEQID NO:2) (ATCC® PTA-6967) were cultured in the Alpha-MEM medium based on the recipe from Dr. Garry Nolan Lab. Cells were maintained in a humidified incubator at 37 °C. SmBiT or LgBiT fusion genes expressed from pDisplay™ were introduced to HeLa cells via Lipofectamine 3000 (Invitrogen). NK-CD16 cells were transduced based on the protocol described elsewhere[11]. Briefly, the Phoenix-AMPHO cells were transfected with the engineered vector (PBMN-IRES-EGFP-SmBiT) via Lipofectamine 3000 to produce recombinant retrovirus. The retroviral supernatant was collected from transfected Phoenix-AMPHO cells for NK-CD16 transduction. NK-CD16 cells with positive SmBiT expression were selected via cell sorting by probing HA tag (anti-HA antibody [Invitrogen #26183, 1:500]; Anti-mouse secondary antibody Alexa Fluor 647 [Invitrogen #A-21235, 1:200]), probing CD16 (anti-CD16 antibody [Abcam #246222, 1:600]; Anti-rabbit secondary antibody Cy3 [Abcam #6939, 1:200]), and probing eGFP simultaneously.

SmBiT/LgBiT Expressions on HeLa Cells

HeLa cells were transfected with pDisplay-LgBiT plasmids (LgBiT-0, 1, 3, and 12 L) via Lipofectamine 3000 (Invitrogen). Transfected cells were harvested at 96 hour post-transfection, suspended in Opti-MEM, and transferred to a 96-well plate (1×10^5 cells per well). HiBiT control protein, a 11 amino acid peptide with a higher affinity to LgBiT than SmBiT (0.7 nM vs. 190 μM), was used to detect LgBiT expression. NanoLuc substrate (furimazine) solution (1:50 diluted) containing 40 nM HiBiT control protein was added to the 96-well plate (20 μL per well). The luminescence was measured at 460 nm by Cytation 3 equipped with 460/40 nm bandpass filter.

The membranous and cytosolic LgBiT and SmBiT proteins were extracted from LgBiT-positive, SmBiT-positive, and HeLa WT cells using Mem-PER Plus membrane protein extraction kit. SmBiT expression was detected by LgBiT proteins. Membranous and cytosolic protein solutions were added to 96-well plates after adjusting the protein level. HiBiT-containing (40 nM) or LgBiT-containing (1:100 diluted) furimazine solution to detect LgBiT or SmBiT proteins.

To evaluate the binding function of the engineered SmBiT and LgBiT proteins at absence of cellular spatial limitations, HeLa cells were co-transfected or separately transfected by pDisplay-SmBiT and pDisplay-LgBiT genes via Lipofectamine 3000 (Invitrogen). Transfected cells were harvested at 96 hour post-transfection, suspended in Opti-MEM, and transferred to a 96-well plate (1×10^5 cells per well). Furimazine solution was added to each well (1:50 diluted, 20 μL per well) 5-min before bioluminescence measurement with Cytation 3.

To test engineered SmBiT-LgBiT protein binding function with the cellular spatial limitations, HeLa cells separately expressed pDisplay-SmBiT or pDisplay-LgBiT 1:1 mixed, transferred to a 96-well plate, and briefly centrifuged at 200g before adding the furimazine solutions. The luminescence was measured at 460 nm by Cytation 3.

SmBiT Expression on NK Cells

SmBiT expression on NK-CD16-SmBiT cells was assessed in addition to HA^+ sorting. NK-CD16-SmBiT cells were transferred to a 96-well plate (1×10^5 cells per well). HeLa transfected with pDisplay-SmBiT genes (SmBiT-0L, 1L, 3L, and 12L) via Lipofectamine 3000 (Invitrogen) worked as positive controls. HeLa WT and NK-CD16 WT cells were used as negative controls. LgBiT-containing (1:100 diluted) furimazine solution was added to $SmBiT^+$ cells to detect SmBiT expression levels. The S/N ratios were calculated as below:

$$\text{S/N ratio} = \frac{\text{NK}_{\text{CD16}}^{\text{SmBiT}}}{\text{NK}_{\text{CD16}}^{\text{WT}}} \text{ or } \frac{\text{HeLa}_{\text{CD16}}^{\text{SmBiT}}}{\text{HeLa}_{\text{CD16}}^{\text{WT}}} \quad \text{(Eq. 1)}$$

LgBiT expression on $CD20^+$ HeLa Cells

CD20 gene (Addgene plasmid # 1890, (van den Heuvel, 1993 #14)) and pDisplay-LgBiT genes (LgBiT-0L, 1L, 3L, and 12L) were introduced to HeLa cells via Lipofectamine 3000 (Invitrogen). Transfected cells were harvested at 96 hour post-transfection. To determine CD20 expressions, transfected and WT Hela cells were washed with PBS, then incubated with FITC anti-CD20 antibody solution (BD B556632, 1:300 dilution) for 30min. Each replicate included 1×10^5 cells. After washing with PBS, FITC signal was quantified using Cytation 3 fluorescence monochromator at λex/em = 485/528 nm with a gain of 100. To determine LgBiT expressions, transfected and WT Hela cells were washed with PBS then suspended in Opti-MEM medium (1×10^5 cells per replicate). NanoLuc substrate (furimazine) solution (1:50 diluted) containing 40 nM HiBiT control protein was added (20 μL per replicate). S/N ratios of CD20 and LgBiT expressions were calculated as Eq. 1.

Antibody-induced effector and target cell-cell interactions in suspension

The ability of the biosensor system to detect antibody-induced cell clustering was validated in HeLa-EGFR:cetuximab:NK system. HeLa cells were transfected by pDisplay-LgBiT-12L cells via Lipofectamine 3000 (Invitrogen). NK-CD16-SmBiT-12L cells were mixed with pDisplay-LgBiT-12L- HeLa cells at E:T ratios of 10 or 5 (1×10^5: 1×10^4 or 5×10^4: 1×10^4 cells in 100 µL medium per well), with or without cetuximab (MedChemExpress) at concentration of 10 nM. NK-CD16 WT cells were mixed with pDisplay-LgBiT-12L-HeLa cells at the same conditions. After 30-min incubation, the luminescence was measured at 460 nm by Cytation 3.

Imaging cell-cell interaction in a 3D cell culture system

At 96 hour post-transfection, $CD20^+LgBiT^+$ HeLa cells were harvested suspended in a 1:1 mixture of Matrigel (BD Bioscience). Matrigel-encapsulated cells were seeded in 24-well plates (20 µL in each well) and solidified at 37 °C for 30 min. In the 3D cell culture imaging studies, NK-CD16 cells with or without SmBiT expression were added to solidified 3D cell cultures with or without rituximab. The images were acquired at 30-min after substrate supplement (furimazine, 1:100 dilution) using an IVIS optical imaging system (Caliper Life Sciences) with an electron multiplying charge-coupled device camera. Acquired images were processed and quantified using Living image 4.5.2 (Caliper Life Sciences).

To compare the sensitivities in detecting rituximab-induced cell clustering betwen LgBiT-3L+SmBiT-12L and LgBiT-12L+SmBiT-12L, corrected bioluminescent signals were calculated as below:

Corrected BLI signal =

$$(\mathrm{NK}_{\mathrm{CD16}}^{\mathrm{SmBiT}}[\mathrm{CTX}] - \mathrm{NK}_{\mathrm{CD16}}^{\mathrm{SmBiT}}[\mathrm{control}]) - (\mathrm{NK}_{\mathrm{CD16}}^{\mathrm{WT}}[\mathrm{CTX}] - \mathrm{NK}_{\mathrm{CD16}}^{\mathrm{WT}}[\mathrm{control}]) \quad \text{(Eq. 2)}$$

The peak corrected signals of each spacer combinations (LgBiT-0L+SmBiT-0L, LgBiT-1L+SmBiT-1L, LgBiT-3L+SmBiT-3L, LgBiT-0L+SmBiT-12L, LgBiT-1L+SmBiT-12L, LgBiT-3L+SmBiT-12L, and LgBiT-12L+SmBiT-12L) were calculated and normalized by control group signals:

$$\text{Normalized signal} = \frac{\text{Corrected BLI signal}}{\mathrm{NK}_{\mathrm{CD16}}^{\mathrm{SmBiT}}[\mathrm{control}]} \quad \text{(Eq. 3)}$$

Results

Proximity-based biosensor system by engineering structurally complementary NanoBiT

The proximity-based biosensor system was engineered from NanoBiT, a complementary structural system composed of a Large BiT (LgBiT, 18 kDa) and a Small BiT (SmBiT, 11 amino acid peptide), which can come together to form an active NanoLuc and generate bright luminescent signals. LgBiT and SmBiT were respectively expressed on target and effector cell membranes. Upon the LgBiT+ and SmBiT+ cell-cell contact, the two complementary parts on opposing cell surfaces come together and emit bright luminescent signals upon the addition of NanoLuc substrate.

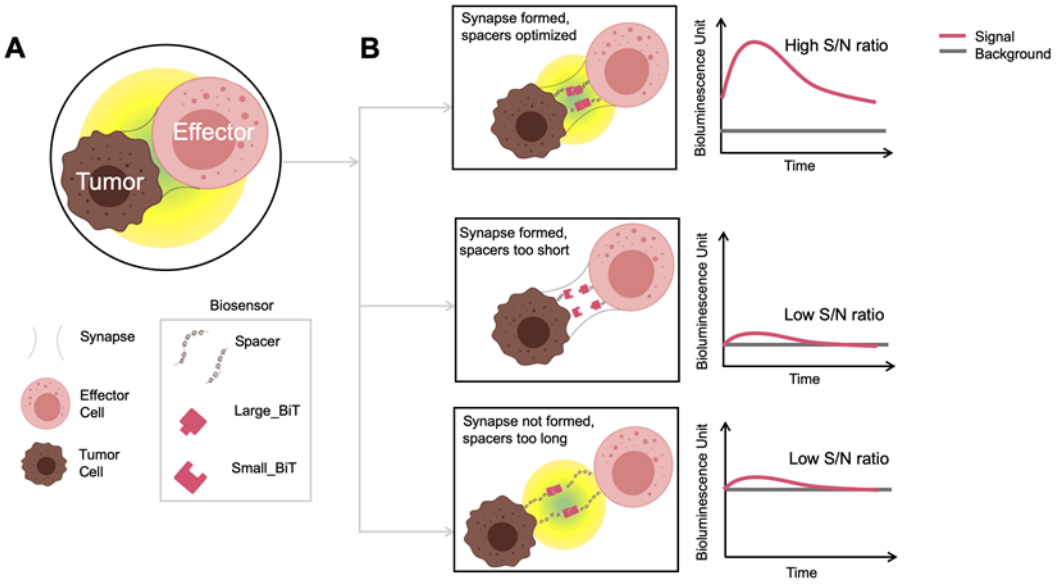

Figure 2: A proximity-based luminescent biosensor system can be used to detect immune: target cell dynamic interactions with optimized selectivity and sensitivity. (A) The schematic of the biosensor system. Briefly, two structurally complementary luciferase subunits in the NanoBiT® system, Large_BiT and Small_BiT, were separately anchored to the surfaces of immune cells and tumor cells by the spacers with various lengths. Once immunological synapses are formed, the proximity between tumor and immune cells allows integration of Large_BiT and Small_BiT, forming active luciferases that emit strong luminescence upon stimulus. The spacer–(GGGGS)n– was selected in constructing the biosensor system for its flexibility, stability, and linearity. The length of the GGGGS spacer is 1.9 nm per unit. (B) Optimizing the sensitivity and selectivity of the biosensor system by adjusting combined spacer lengths. The biosensor system subunits have different spacer lengths, facilitating the optimization of the signal-to-noise (S/N) ratios. When combined spacer lengths were too short, the sensitivity of detection by the biosensor system will decrease (middle panel). When combined spacer lengths were too long, the biosensor system will create high background signal and reduce the selectivity in detecting the formation of immunological synapses (lower panel).

The molecular bonds between LgBiT and SmBiT did not noticeably interfere with the natural intercellular interaction between effector and target cells, due to their low binding affinity (190 μM). Spacers with different lengths were fused to NanoBiT to optimize the system with sufficient detecting sensitivity and selectivity (Figure 1 and Figure 2A). Spacer-fused SmBiT biosensor components were constructed in plasmid DNA and viral vector forms. We tested the biosensor system with a wide range of combined spacer lengths from 0 – 48 nm (Table 10), and the optimized spacer lengths were then determined for given pair of effector and target cells with the highest S/N ratios (Figure 2B, upper panel). When combined spacer lengths were too short, the sensitivity of detection by the biosensor system decreased (Figure 2B, middle panel). When combined spacer lengths were too long, the biosensor system would show high noise (i.e.,

background signal) with reduced selectivity for detecting stable cell-cell interaction (Figure 2B, lower panel).

TABLE 1 Construction of the biosensor system

LgBiT		SmBiT	
Biosensor subunit structure	Spacer length (nm)	Biosensor subunit structure	Spacer length (nm)
N'– LgBiT – C'	0	N'– SmBiT – C'	0
N'–LgBiT –$(GGGGS)_1$ –C'	2	N'–SmBiT –$(GGGGS)_1$ –C'	2
N'–LgBiT –$(GGGGS)_3$ –C'	6	N'–SmBiT –$(GGGGS)_3$ –C'	6
N'–LgBiT –$(GGGGS)_{12}$ –C'	24	N'–SmBiT –$(GGGGS)_{12}$ –C'	24

Engineered biosensor system detected cell-cell interactions with high sensitivity

We characterized the expressions and functions of the biosensor system on HeLa cell surfaces. As Figure 3A shows, the LgBiT expression in HeLa cells was several orders of magnitude higher than background ($p < 0.0001$, unpaired Student's t-test). The expression of SmBiT in HeLa cells detected by HA probing was significant ($p < 0.0001$, unpaired Student's t-test). We then investigated the cellular location of LgBiT and SmBiT. Despite LgBiT and SmBiT expressions were detetable in cytosols (Figure 3B and 38C), both were majorly expressed on cell membranes. LgBiT had approximately 40-fold higher expression on cell membrane than in cytosols ($p = 0.0006$, unpaired Student's t-test). Membranous SmbiT expression was more than ten times higher than cytosolic SmBiT ($p = 0.02$, unpaired Student's t-test). High membranous expressions make it suitable for detecting intercellular interactions (Figure 3B).

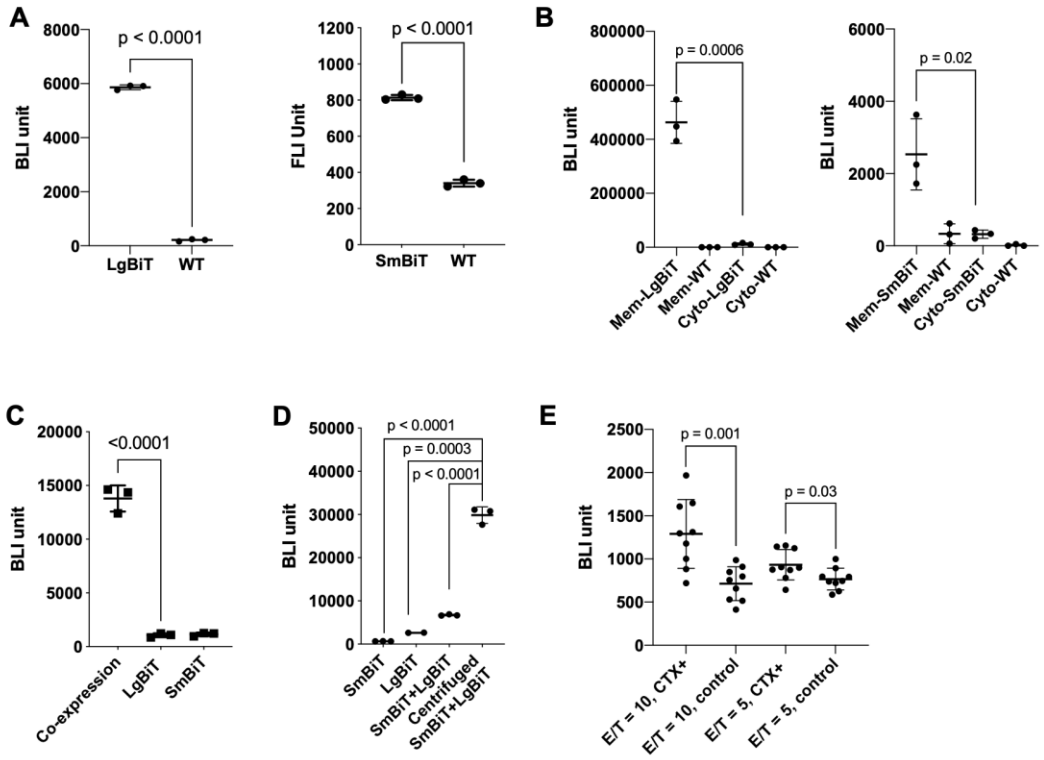

Figure 3: Engineered biosensor system detected cell-cell interactions with high sensitivity. (A) LgBiT and SmBiT were successfully expressed in HeLa cells as indicated by HiBiT probing (Left panel, $p < 0.0001$, unpaired Student's t-test) or HA tag probing (Right panel, $p < 0.0001$, unpaired Student's t-test). (B) LgBiT and SmBiT were majorly

expressed on cell membranes. Left panel: Compared to HeLa WT cells, LgBiT expression on membrane and in cytosol were significantly elevated ($p = 0.0005$ and $p = 0.007$, unpaired Student's t-test). Membranous LgBiT expression was substantially higher than cytosolic expression ($p = 0.0070$, unpaired Student's t-test). Right panel: Compared to HeLa WT cells, SmBiT expression on membrane and in cytosol were significantly elevated ($p = 0.02$ and $p = 0.01$, unpaired Student's t-test). Membranous SmBiT expression was substantially higher than cytosolic expression ($p = 0.02$, unpaired Student's t-test). (C) Co-expressed LgBiT and SmBiT emitted strong luminescent signals compared to LgBiT- or SmBiT-positive cells alone ($p < 0.0001$, unpaired Student's t-test). (D) Biosensor system detected cell contacts that elevated by centrifugation. Compared to centrifuged LgBiT- or SmBiT-positive cells alone and uncentrifuged LgBiT:SmBiT cell mixtures, the bioluminescent signals of centrifugated LgBiT:SmBiT cell mixtures increased significantly ($p = 0.0003$, $p < 0.0001$, and $p < 0.0001$, unpaired Student's t-test). (E) Hela: NK-CD16 interactions were elevated by anti-EGFR antibody cetuximab. The bioluminescent signals were measured after 30-min incubation of Hela and NK-CD16, with or without cetuximab. Cetuximab elevated bioluminescent signals significantly in both E/T= 10 group and E/T= 5 group ($p = 0.001$ and $p = 0.03$, unpaired Student's t-test). Cetuximab-specific signals were higher in E/T= 10 group than E/T= 5 group ($p = 0.03$, unpaired Student's t-test). From (A) to (E), each data point represents one technical replicate. Error bars represent SD values. At least three independent biologic replicates were performed per experiment. MEM = membranous; cyto = cytosolic; E/T = effector/target cell ratio; WT = wild type.

We then characterized the interacting probability LgBiT and SmBiT using different cell systems. When co-expressed on cell membrane, bound LgBiT-SmBiT emitted strong luminescent signals (Figure 3C), while LgBiT- or SmBiT-positive cells alone had negligible background signals. When SmBiT and LgBiT expressed on the same cells (without spatial restriction), strong bioluminescence signal was detected. When SmBiT and LgBiT expressed on separate cell membrane ($SmBiT^+$ and $LgBiT^+$ HeLa cells), the bioluminescent signal was low when two cell types were both in suspension (Figure 3D). We increased the intercellular interacting probability by centrifugation. Compared to cell suspension, the bioluminescent signals of centrifugated LgBiT:SmBiT cell mixtures increased by 5 – 10 times (Figure 3D), suggesting the detecting signal is intercellular contact-dependent.

We then used the biosensor system to investigate antibody-specific cell-cell interactions. Intercellular interaction between NK-CD16 and Hela cells induced by anti-EGFR antibody cetuximab was first evaluated. $SmBiT^+$ NK-CD16 cells were incubated with $LgBiT^+$ HeLa cells at different E:T ratios (5 or 10), with or without cetuximab (Figure 3E). Without cetuximab, no significantly different bioluminescent signals were detected in the effector-target cell mixtures regardless E:T ratios ($p = 0.5$, unpaired Student's t-test). Cetuximab significantly increased effector-target cell interactions ($p = 0.001$ and $p = 0.03$, unpaired Student's t-test). The bioluminescent signals were significantly higher in the 10 E:T ratio group than the group with 5 E:T ratio ($p = 0.02$, unpaired Student's t-test).

Visualizing cell-cell interaction between effector and target cells in a 3D cell culture system

Intercellular interactions between NK-CD16 and $CD20^+$HeLa cells induced by rituximab were evaluated in the 3D cell culture system. NK-CD16 cells transfected with SmBiT with different linker lengths (SmBiT-0L, SmBiT-1L, SmBiT-3L, and SmBiT-12L cells) had comparable CD16 and HA expression levels (Figure 4A and Figure 1). All four $SmBiT^+$NK-CD16 cell lines (SmBiT-0L, SmBiT-1L, SmBiT-3L, and SmBiT-12L) had substantially higher SmBiT expressions than positive controls (Figure 4B). No significant difference in SmBiT expressions among the four $SmBiT^+$NK-CD16 cell lines was observed ($p = 0.1$, ordinary one-way ANOVA). CD20 expression levels were largely comparable among $CD20^+LgBiT^+$ HeLa cell lines (LgBiT-0L, LgBiT-1L, LgBiT-3L, and LgBiT-12L cells) (Figure 4C). HeLa cells had relatively lower

expressions of LgBiT-0L and LgBiT-1L and the expressions of LgBiT-3L and LgBiT-12L were comparable (Figure 4C).

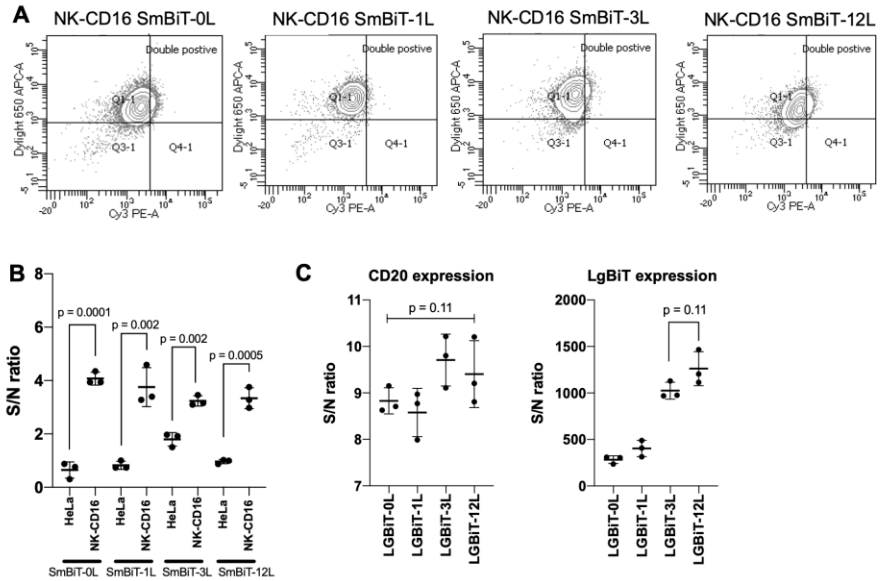

Figure 4: Constructing biosensor system in NK-CD16 and CD20+HeLa cells. (A) NK-CD16 cells stably expressing SmBiT (SmBiT-0L, SmBiT-1L, SmBiT-3L, and SmBiT-12L) were sorted by HA tag (Dylight 650) and CD16 (Cy3). (B) SmBiT expression in SmBiT-0L, SmBiT-1L, SmBiT-3L, and SmBiT-12L were comparable ($p = 0.1$, ordinary one-way ANOVA) and significantly higher than positive controls, i.e., HeLa cells transiently-expressing SmBiT ($p = 0.0001$, $p = 0.002$, $p = 0.002$, and $p = 0.0005$, unpaired Student's t-test). (C) CD20 expressions were comparable between CD20+LgBiT+ HeLa cell lines (LgBiT-0L, LgBiT-1L, LgBiT-3L, and LgBiT-12L cells, $p = 0.11$, ordinary one-way ANOVA). (D) LgBiT expression in CD20+LgBiT+ HeLa cell lines. No significant difference was observed in LgBiT expression in LgBiT-3L and LgBiT-12L cells. $p = 0.11$, unpaired Student's t-test). In (B) and (C), each data point represents one technical replicate. Error bars represent SD values. At least three independent biologic replicates were performed per experiment.

We imaged rituximab-induced NK-CD16 and CD20^{+}HeLa interactions using LgBiT-12L: SmBiT-12L pair in the 3D cell culture system for 48 hours (Figure 5). Figure 5B showed the real-time NK-CD16 and CD20^{+}HeLa interactions in the 3D The bioluminescent signals were relatively low at the beginning of the imaging study (0.5 hr), then increased and peaked around the 2.5 hour, suggesting increasing frequency of effector and target cell interactions over time (Figure 5A). Their interactions decreased from 2.5 to 9 hour.

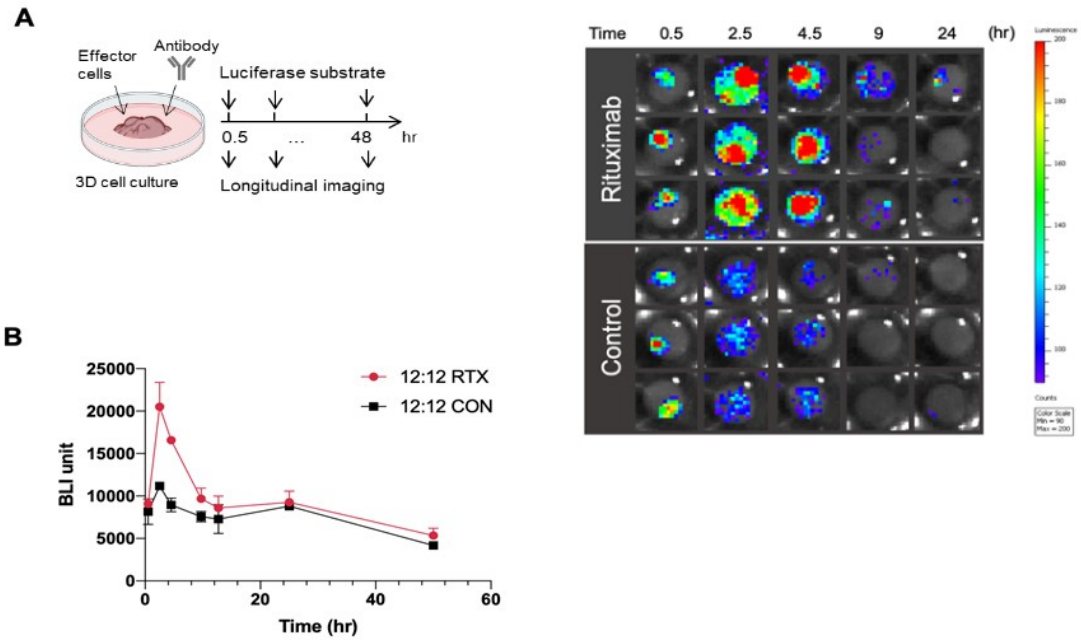

Figure 5: Visualizing NK-CD16 and CD20+HeLa interactions in 3D cell cultures. (A) Study design and bioluminescent images of NK-CD16 and CD20+HeLa interactions at 0.5, 2.5, 4.5, 9, and 24 hour. RTX = rituximab; CON = control. (A) Bioluminescent intensity revealing direct interaction between NK-CD16 and CD20+HeLa cells. LgBiT-12L: SmBiT-12L pair was used. Each data point represents one technical replicate. Error bars represent SD values. At least three independent biologic replicates were performed per experiment.

Optimizing the biosensor system in a 3D cell culture system

We selected the biosensor pair with optimal sensitivity by evaluating the peak rituximab-specific signals from LgBiT$^+$NK-CD16: SmBiT$^+$CD20$^+$HeLa cell interactions in 3D cell cultures (Figure 6A). Given the varying expressions of LgBiT in CD20$^+$LgBiT$^+$ HeLa cells (Figure 3C), rituximab-specific signals were normalized by the peak signals from the control group. The biosensor pair with the shortest theoretical combined spacer length (LgBiT-0L+ SmBiT-0L) had the lowest rituximab-specific signal. The pair with the longest theoretical combined spacer length (LgBiT-12L: SmBiT-12L) had the highest rituximab-specific signal. The selectivity was also assessed. The rituximab-specific signals increased as the combined spacer lengths increased from 0 to 12 nm (i.e., LgBiT-0L: SmBiT-0L, LgBiT-1L: SmBiT-1L, and LgBiT-3L: SmBiT-3L. Figure 6A). Interestingly, we found that the combined spacer length was not the only factor influencing the detecting selectivity. The LgBiT-0L: SmBiT-12L pair had much lower rituximab-specific signals than the LgBiT-3L: SmBiT-3L pair ($p = 0.005$, unpaired Student's t-test). The biosensor pairs with different combined spacer lengths, e.g., LgBiT-3L: SmBiT-3L, LgBiT-1L: SmBiT-12L, and LgBiT-3L: SmBiT-12L, had comparable rituximab-specific signals ($p = 0.9$, one-way ANOVA).

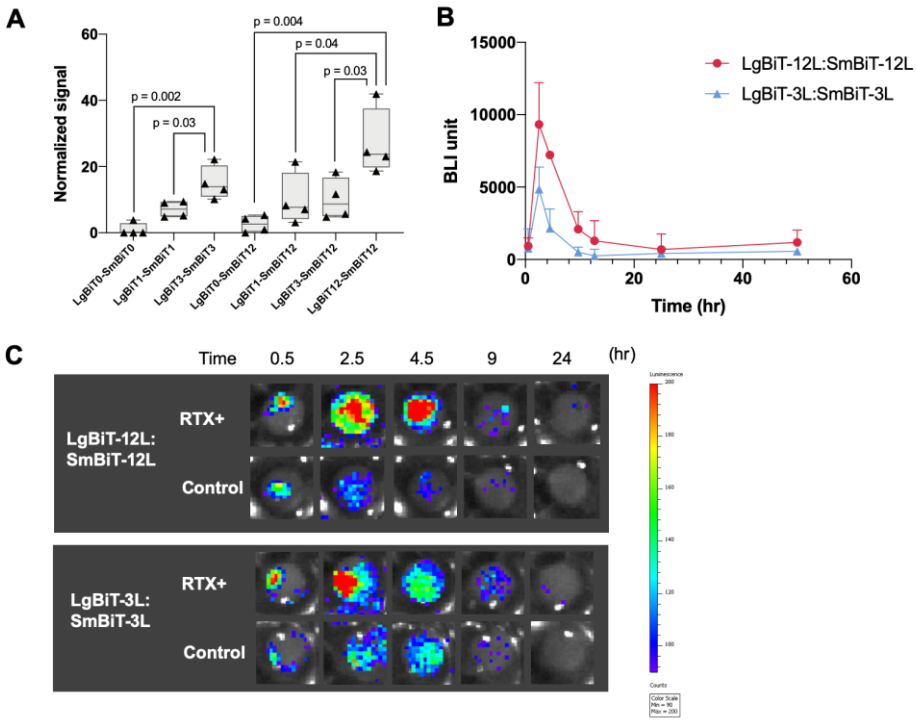

Figure 6: Optimizing selectivity and sensitivity of the biosensor system in 3D cell cultures. (A) LgBiT-12L: SmBiT-12L pair showed the optimal sensitivity compared to other pairs. LgBiT-3L: SmBiT-3L pair showed higher normalized rituximab-specific signals than LgBiT-0L: SmBiT-0L and LgBiT-1L: SmBiT-1L pairs ($p = 0.002$ and $p = 0.03$, unpaired Student's t-test). LgBiT-12L: SmBiT-12L pair showed higher normalized rituximab-specific signals than LgBiT-0L: SmBiT-12L, LgBiT-1L: SmBiT-12L, and LgBiT-3L: SmBiT-12L pairs ($p = 0.004$, $p = 0.04$, and $p = 0.03$, unpaired Student's t-test). (B) Corrected bioluminescent signals indicated LgBiT-12L: SmBiT-12L pair showed higher selectivity than LgBiT-3L: SmBiT-3L pair. In (A) and (B), each data point represents one technical replicate. Error bars represent SD values. At least three independent biologic replicates were performed per experiment. (C) Bioluminescent images of NK-CD16 and $CD20^{+}$HeLa interactions at 0.5, 2.5, 4.5, 9, and 24 hour. RTX = rituximab.

The LgBiT-3L: SmBiT-3L and LgBiT-12L: SmBiT-12L biosensor pairs were used to demonstrate system sensitivity in detecting antibody-specific signals (Figure 6B, 41C, and 39C). Compared to the LgBiT-12L: SmBiT-12L biosensor pair, LgBiT-3L: SmBiT-3L biosensor pair had lower rituximab-specific signals (Figure 6B). The relatively lower sensitivity of LgBiT-3L: SmBiT-3L biosensor pair compared to LgBiT-12L: SmBiT-12L pair in detecting rituximab-induced cell-cell interaction was also observed in longitudinal imaging (Figure 6C and Figure 7). LgBiT-12L: SmBiT-12L biosensor pair was then selected for the subsequent imaging in the 3D culture system.

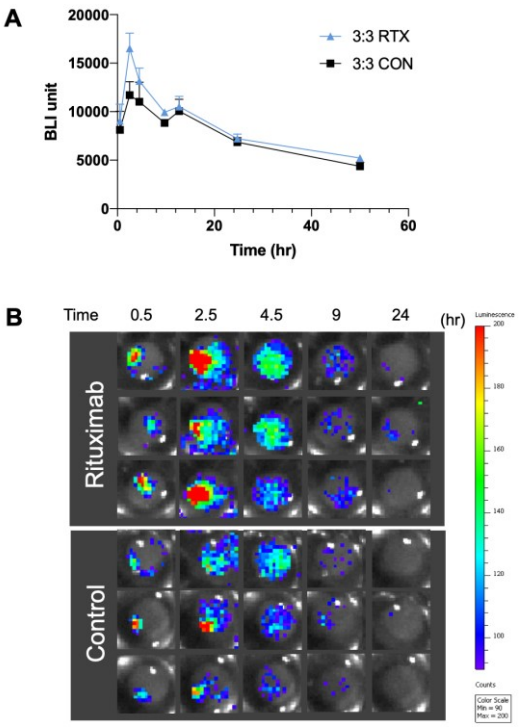

Figure 7: LgBiT-3L: SmBiT-3L pair showed less sensitivity in detecting NK-CD16 and CD20^{+}HeLa interactions compared to LgBiT-12L: SmBiT-12L pair. (A) Raw data of bioluminescent signals from NK-CD16 and CD20^{+}HeLa interactions. LgBiT-3L: SmBiT-3L pair was evaluated. Each data point represents one technical replicate. Error bars represent SD values. At least three independent biologic replicates were performed per experiment. (B) Bioluminescent images of NK-CD16 and CD20^{+}HeLa interactions at 0.5, 2.5, 4.5, 9, and 24 hour. RTX = rituximab; CON = control.

Intercellular Interaction induced by rituximab was antibody concentration-dependent

We investigated antibody-induced effector: target intercellular interaction at different rituximab concentrations (1 and 100 µg/mL). As shown in Figure 8, antiody-induced signal peaked at 2 hour in both dose groups, similar to the previous observations (Figures 5 and 6). Compared to the low dose group, the high dose group (100 µg/mL) had substantially higher cell-cell interaction throughout the imaging window (Figure 8B), suggesting antibody concentration-dependent cell-cell interactions.

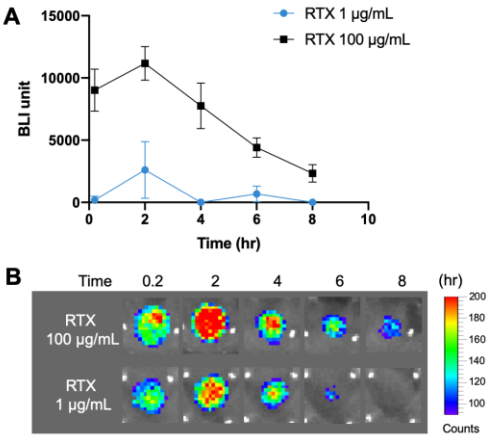

Figure 8: Rituximab-induced effector: target cell clustering was antibody concentration-dependent. Raw data of bioluminescent signals from NK-CD16 and CD20^{+}HeLa interactions, which was visualized by LgBiT-12L: SmBiT-12L pair. Each data point represents one technical replicate. Error bars represent SD values. At least three independent biologic replicates were performed per experiment. (B) Bioluminescent images of NK-CD16 and CD20^{+}HeLa interactions at 0.2, 2, 4, 6, and 8 hour. RTX = rituximab.

Intercellular Interaction induced by blinatumomab

Intercellular interactions between c induced by a bispecific T cell engaging antibody blinatumomab was also assessed using the system. Similarly, we tested the system sensitivity and selectivity by comparing the signals across a range of linker lengths. Interestingly, the optimal linker pair was found to be LgBiT-3L: SmBiT-3L, shorter than the optimal length for NK and target cell interactions. As shown in Figure 9, blinatumomab-induced T and target cell interactions peaked at 6 hours, slower than rituximab-induced NK and target cell interactions.

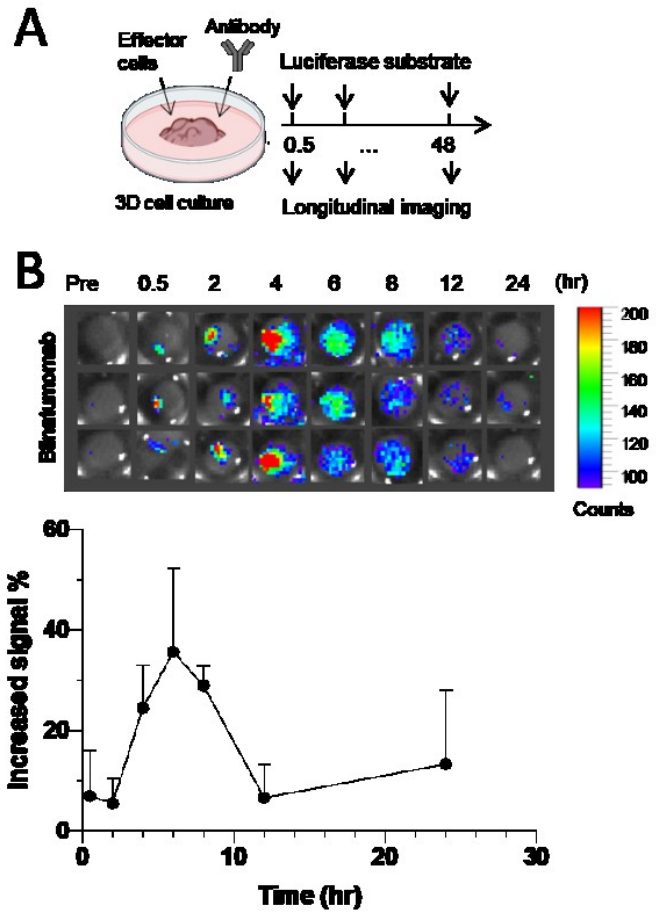

Figure 9: Blinatumomab-induced T: target cell interaction Raw data of bioluminescent signals from Jurkat T (CD3+) and Raj B (CD19) cell-cell interactions in the 3D cell culture system, which was visualized by LgBiT-3L: SmBiT-3L pair. Each data point represents one technical replicate. Error bars represent SD values. At least three independent biologic replicates were performed per experiment. (B) Bioluminescent images of at 0.2, 2, 4, 6, and 8 hour at 1 ng/ml blinatumomab.

Discussion

Activating ADCC by NK cells is an essential mechanism of action for many therapeutic antibodies, especially the ones treating cancers. More than 10 FDA-approved antibodies have shown ADCC effects, and the trend of antibody engineering focused on the improvement of antibody effector function is expected to continue[12]. The mechanisms of ADCC have been extensively studied in vitro. ADCC is initiated with immune: target cell conjugation and immunological synapse formation[13]. NK cells encounter and recognize the target cells opsonized by antibodies, forming a firm adhesion to the target cell and a stable NK-target cell interface with a 'cleft,' into which cytolytic molecules are secreted to eradicate the target cells[13]. There is good evidence that ADCC is involved with cancer treatment responses in animal models and patients[14-18]. However, the mechanisms of ADCC in vivo and the contribution of ADCC to antibody treatment responses have not been completely understood; most measurements of ADCC consist of bulk assays or discontinuous methods, obscuring the spatial and temporal resolutions of ADCC effects and lacking the physiological context. Tools that noninvasively assess ADCC in the living system are highly desired, especially in the tumor microenvironment.

We developed a proximity-based biosensor system to detect the initial NK: target cell conjugation in ADCC effects and continuously monitor cell-clustering dynamics. We expressed structural complementary luciferase subunits to the opposing NK and target cells to indicate cell conjugation via strong and bright bioluminescent signals. To optimize the selectivity and sensitivity of the biosensor system, we equipped the split luciferases with different lengths of spacer to capture the distances between the opposing membranes in NK-target cell synapse, which are believed to be 15 – 40 nm[19,20]. The spacer –(GGGGS)n– was selected to construct the biosensor systems for flexibility, stability, and linearity[21]. The biosensor system detected the cell contacts with high sensitivity and successfully captured the elevated signals from antibody-induced NK-target cell interactions (Figure 3D and E).

We evaluated the NK-target cell conjugation induced by rituximab, an anti-CD20 antibody that mainly elicits treatment effects via ADCC, in 3D cell cultures that mimic the physiological conditions in solid tumors and minimize the interference of shear force on cell conjugations[22-24]. The temporal change of NK-target interactions was visualized by robust bioluminescent signals (Figure 5). We observed dynamic bioluminescent signals from the control group (Figure 5), which indicated that NK-CD16 cells interacted with target cells without rituximab. This non-antibody-specific cell conjugation is possibly mediated by other receptors such as IL2R[25-29].

The rituximab group's significantly higher yet simultaneous peak signals compared to the control group indicated that rituximab increased NK: target cell conjugation frequencies rather than substantially shifting the cell conjugation dynamics (Figure 5). Similar findings were observed in the cell conjugation kinetics at different rituximab concentrations (Figure 8). These findings agreed with previous studies[30,31]. Another interesting finding was that the cell conjugation peaked at around 2 hours. This peak time may result from the rituximab and NK cell distribution kinetics. While rituximab can opsonize the target cells rapidly, NK cell trafficking to the 3D culture in a closed system could be relatively slower[32,33]. Another possible explanation is the sequential killing effects of NK cells[34-38]. A single NK cell can sequentially attack the next targets. Choi and colleagues described the bursting kinetics of NK cells by time-lapse single-cell imaging technology, in which a slow initial kill followed by subsequent rapid kills was described. Establishing the first cell conjugate was around 80 mins for most NK cells[34]. The following killing events were frequent within 1 – 4 hours[37]. Those observations agreed with our findings (Figure 5 and Figure 7).

We observed that the biosensor system's selectivity and sensitivity did not solely depend on linker length (Figure 6). The biosensor pairs with inflexible split luciferase components (i.e., no spacer, LgBiT-0L) had the lowest S/N ratios regardless of the theoretical combined spacer lengths (Figure 6), suggesting that certain degrees of flexibility of the biosensor system are required to detect cell interactions. Yielding approximately 12, 26, and 30 nm theoretical combined spacer lengths (LgBiT-3L: SmBiT-3L, LgBiT-1L: SmBiT-12L, and LgBiT-3L: SmBiT-12L, respectively), which are close to the theoretical distances between opposing cell membranes in a synapse (15 – 40 nm), the biosensor pairs showed similar rituximab-specific bioluminescent signals. The pair with longer theoretical combined spacer lengths did not offer superior sensitivity (Figure 6A). These observations could possibly be explained by the unstable distances between the opposing cell membranes in synapses. Rather than rigid surfaces, cell membranes in the synapse are constantly moving and changing along with synapse formation progress. The weak binding (190 μM) between the luciferase subunits in the biosensor system can be easily interrupted by the membrane movement even though the biosensor pairs' theoretical combined spacer lengths were adequate, limiting the detection sensitivity. LgBiT-12L: SmBiT-12L pair provided the highest sensitivity in detecting cell conjugations, possibly due to the proper flexibility on both sides.

We showed that the proximity-based biosensor system allowed a continuous and noninvasive observation of antibody-induced cell clustering dynamics in tumor-like 3D cell cultures. The biosensor system robustly detected signals arising from antibody-specific cell conjugations at low target cell levels (less than 0.5 million), which was substantially lower than the cell numbers in real solid tumors (at least 1,000 million)[39], demonstrating the great potential of applying this biosensor system in detecting cell clustering dynamics in vivo. Moreover, we showed that the biosensor system's selectivity and sensitivity could be optimized based on synapse sizes. This feature detects synapses induced by other treatment modalities, such as T-cell: tumor cell conjugation caused by bispecific T-cell engagers. Our studies have several limitations. Firstly, antibody and NK cell distribution kinetics in the 3D cell culture was not investigated. The antibody-specific NK: target cell conjugation could be restricted at the periphery of 3D culture due to the slow antibody distribution rate in the tumor-like matrix. Secondly, the NK: target cell clustering dynamics were measured in a closed system, which did not incorporate the complex physiological factors, including antibody pharmacokinetics, NK cell distribution kinetics, and the influences of the intricate solid tumor microenvironment. Thirdly, we did not establish the relationship between cell conjugation and cell-killing effects. Further studies are warranted.

Funding Source: National Institute of Health, R35GM119661

Author Contributions

Conceptualizations: Y.T., and Y.C.; methodology: Y.T., and Y.C.; formal analysis: Y.T., and Y.C.; investigation: J Y.T., and Y.C.; writing-original draft: Y.T., and Y.C.; writing-reviewing and editing: Y.T., and Y.C.; supervision: Y.C.

Competing Interests

All the authors declare no competing interests.

Correspondence and requests for materials should be addressed to Y.C.

Reference

1. Patrick Chames, Marc Van Regenmortel, Etienne Weiss, and Daniel Baty. Therapeutic antibodies: successes, limitations and hopes for the future. Br J Pharmacol. 2009 May; 157(2): 220–233.
2. Yu Tang, Yanguang Cao Modeling Pharmacokinetics and Pharmacodynamics of Therapeutic Antibodies: Progress, Challenges, and Future Directions. Pharmaceutics. 2021; 13(3): 422.
3. Alex D Waldman, Jill M Fritz, Michael J Lenardo. A guide to cancer immunotherapy: from T cell basic science to clinical practice. Nat Rev Immunol. 2020;20(11):651-668. doi: 10.1038/s41577-020-0306-5
4. Sarah E Shelton, Huu Tuan Nguyen, David A Barbie, Roger D Kamm. Engineering approaches for studying immune-tumor cell interactions and immunotherapy. iScience. 2021; 24(1): 101985.
5. Tyler J Bechtel, Tamara Reyes-Robles, Olugbeminiyi O Fadeyi, Rob C Oslund. Strategies for monitoring cell–cell interactions. Nat Chem Biol. 2021. PMID: 34035514.
6. Sarah E Shelton, Huu Tuan Nguyen, David A Barbie, Roger D Kamm. Engineering approaches for studying immune-tumor cell interactions and immunotherapy. iScience. 2021 Jan 22; 24(1): 101985.
7. Zhang D, He W, Wu C, Tan Y, He Y, Xu B, Chen L, Li Q, Jiang J. Scoring System for Tumor-Infiltrating Lymphocytes and Its Prognostic Value for Gastric Cancer. Front Immunol. 2019;10:71.
8. Deciphering cell–cell interactions and communication from gene expression. Erick Armingol, Adam Officer, Olivier Harismendy & Nathan E. Lewis. Nature Reviews Genetics volume 22, pages71–88 (2021)
9. Dixon, A.S.; Schwinn, M.K.; Hall, M.P.; Zimmerman, K.; Otto, P.; Lubben, T.H.; Butler, B.L.; Binkowski, B.F.; Machleidt, T.; Kirkland, T.A., et al. NanoLuc Complementation Reporter Optimized for Accurate Measurement of Protein Interactions in Cells. ACS Chem Biol 2016, 11, 400-408, doi:10.1021/acschembio.5b00753.
10. Yang, J.; Zhang, Z.; Lin, J.; Lu, J.; Liu, B.F.; Zeng, S.; Luo, Q. Detection of MMP activity in living cells by a genetically encoded surface-displayed FRET sensor. Biochim Biophys Acta 2007, 1773, 400-407, doi:10.1016/j.bbamcr.2006.11.002.
11. Miah, S.M.; Campbell, K.S. Expression of cDNAs in human Natural Killer cell lines by retroviral transduction. Methods Mol Biol 2010, 612, 199-208, doi:10.1007/978-1-60761-362-6_13.
12. Wang, S.Y.; Weiner, G. Complement and cellular cytotoxicity in antibody therapy of cancer. Expert Opin Biol Ther 2008, 8, 759-768, doi:10.1517/14712598.8.6.759.
13. Barreira da Silva, R.; Graf, C.; Munz, C. Cytoskeletal stabilization of inhibitory interactions in immunologic synapses of mature human dendritic cells with natural killer cells. Blood 2011, 118, 6487-6498, doi:10.1182/blood-2011-07-366328.
14. Chang, H.Y.; Wu, S.; Li, Y.; Zhang, W.; Burrell, M.; Webster, C.I.; Shah, D.K. Brain pharmacokinetics of anti-transferrin receptor antibody affinity variants in rats determined using microdialysis. MAbs 2021, 13, 1874121, doi:10.1080/19420862.2021.1874121

15. Helguera, G.; Rodriguez, J.A.; Luria-Perez, R.; Henery, S.; Catterton, P.; Bregni, C.; George, T.C.; Martinez-Maza, O.; Penichet, M.L. Visualization and quantification of cytotoxicity mediated by antibodies using imaging flow cytometry. J Immunol Methods 2011, 368, 54-63, doi:10.1016/j.jim.2011.03.003.
16. Minard-Colin, V.; Xiu, Y.; Poe, J.C.; Horikawa, M.; Magro, C.M.; Hamaguchi, Y.; Haas, K.M.; Tedder, T.F. Lymphoma depletion during CD20 immunotherapy in mice is mediated by macrophage FcgammaRI, FcgammaRIII, and FcgammaRIV. Blood 2008, 112, 1205-1213, doi:10.1182/blood-2008-01-135160.
17. Cartron, G.; Dacheux, L.; Salles, G.; Solal-Celigny, P.; Bardos, P.; Colombat, P.; Watier, H. Therapeutic activity of humanized anti-CD20 monoclonal antibody and polymorphism in IgG Fc receptor FcgammaRIIIa gene. Blood 2002, 99, 754-758, doi:10.1182/blood.v99.3.754.
18. Musolino, A.; Naldi, N.; Bortesi, B.; Pezzuolo, D.; Capelletti, M.; Missale, G.; Laccabue, D.; Zerbini, A.; Camisa, R.; Bisagni, G., et al. Immunoglobulin G fragment C receptor polymorphisms and clinical efficacy of trastuzumab-based therapy in patients with HER-2/neu-positive metastatic breast cancer. J Clin Oncol 2008, 26, 1789-1796, doi:10.1200/JCO.2007.14.8957.
19. Chakraborty, A.K. How and why does the immunological synapse form? Physical chemistry meets cell biology. Sci STKE 2002, 2002, pe10, doi:10.1126/stke.2002.122.pe10.
20. Cleary, K.L.S.; Chan, H.T.C.; James, S.; Glennie, M.J.; Cragg, M.S. Antibody Distance from the Cell Membrane Regulates Antibody Effector Mechanisms. J Immunol 2017, 198, 3999-4011, doi:10.4049/jimmunol.1601473.
21. Chen, X.; Zaro, J.L.; Shen, W.C. Fusion protein linkers: property, design and functionality. Adv Drug Deliv Rev 2013, 65, 1357-1369, doi:10.1016/j.addr.2012.09.039.
22. Edmondson, R.; Broglie, J.J.; Adcock, A.F.; Yang, L. Three-dimensional cell culture systems and their applications in drug discovery and cell-based biosensors. Assay Drug Dev Technol 2014, 12, 207-218, doi:10.1089/adt.2014.573.
23. Decaup, E.; Rossi, C.; Gravelle, P.; Laurent, C.; Bordenave, J.; Tosolini, M.; Tourette, A.; Perrial, E.; Dumontet, C.; Poupot, M., et al. A Tridimensional Model for NK Cell-Mediated ADCC of Follicular Lymphoma. Front Immunol 2019, 10, 1943, doi:10.3389/fimmu.2019.01943.
24. Schnalzger, T.E.; de Groot, M.H.; Zhang, C.; Mosa, M.H.; Michels, B.E.; Roder, J.; Darvishi, T.; Wels, W.S.; Farin, H.F. 3D model for CAR-mediated cytotoxicity using patient-derived colorectal cancer organoids. EMBO J 2019, 38, doi:10.15252/embj.2018100928.
25. Orange, J.S. Formation and function of the lytic NK-cell immunological synapse. Nat Rev Immunol 2008, 8, 713-725, doi:10.1038/nri2381.
26. Orange, J.S.; Harris, K.E.; Andzelm, M.M.; Valter, M.M.; Geha, R.S.; Strominger, J.L. The mature activating natural killer cell immunologic synapse is formed in distinct stages. Proc Natl Acad Sci U S A 2003, 100, 14151-14156, doi:10.1073/pnas.1835830100.

27. Chen, S.; Kawashima, H.; Lowe, J.B.; Lanier, L.L.; Fukuda, M. Suppression of tumor formation in lymph nodes by L-selectin-mediated natural killer cell recruitment. J Exp Med 2005, 202, 1679-1689, doi:10.1084/jem.20051473.
28. Warren, H.S.; Altin, J.G.; Waldron, J.C.; Kinnear, B.F.; Parish, C.R. A carbohydrate structure associated with CD15 (Lewis x) on myeloid cells is a novel ligand for human CD2. J Immunol 1996, 156, 2866-2873.
29. Inoue, H.; Miyaji, M.; Kosugi, A.; Nagafuku, M.; Okazaki, T.; Mimori, T.; Amakawa, R.; Fukuhara, S.; Domae, N.; Bloom, E.T., et al. Lipid rafts as the signaling scaffold for NK cell activation: tyrosine phosphorylation and association of LAT with phosphatidylinositol 3-kinase and phospholipase C-gamma following CD2 stimulation. Eur J Immunol 2002, 32, 2188-2198, doi:10.1002/1521-4141(200208)32:8<2188::AID-IMMU2188>3.0.CO;2-T.
30. Kamen, L.; Thakurta, T.; Myneni, S.; Zheng, K.; Chung, S. Development of a kinetic antibody-dependent cellular cytotoxicity assay. J Immunol Methods 2019, 468, 49-54, doi:10.1016/j.jim.2019.02.006.
31. Li, G.; Zhang, L.; Chen, E.; Wang, J.; Jiang, X.; Chen, J.H.; Wickman, G.; Amundson, K.; Bergqvist, S.; Zobel, J., et al. Dual functional monoclonal antibody PF-04605412 targets integrin alpha5beta1 and elicits potent antibody-dependent cellular cytotoxicity. Cancer Res 2010, 70, 10243-10254, doi:10.1158/0008-5472.CAN-10-1996.
32. Sriraman, S.K.; Aryasomayajula, B.; Torchilin, V.P. Barriers to drug delivery in solid tumors. Tissue Barriers 2014, 2, e29528, doi:10.4161/tisb.29528.
33. Jain, R.K. Delivery of molecular and cellular medicine to solid tumors. Adv Drug Deliv Rev 2012, 64, 353-365, doi:10.1016/j.addr.2012.09.011.
34. Romain, G.; Senyukov, V.; Rey-Villamizar, N.; Merouane, A.; Kelton, W.; Liadi, I.; Mahendra, A.; Charab, W.; Georgiou, G.; Roysam, B., et al. Antibody Fc engineering improves frequency and promotes kinetic boosting of serial killing mediated by NK cells. Blood 2014, 124, 3241-3249, doi:10.1182/blood-2014-04-569061.
35. Choi, P.J.; Mitchison, T.J. Quantitative analysis of resistance to natural killer attacks reveals stepwise killing kinetics. Integr Biol (Camb) 2014, 6, 1153-1161, doi:10.1039/c4ib00096j.
36. Douglass, E.F., Jr.; Miller, C.J.; Sparer, G.; Shapiro, H.; Spiegel, D.A. A comprehensive mathematical model for three-body binding equilibria. J Am Chem Soc 2013, 135, 6092-6099, doi:10.1021/ja311795d.
37. Choi, P.J.; Mitchison, T.J. Imaging burst kinetics and spatial coordination during serial killing by single natural killer cells. Proc Natl Acad Sci U S A 2013, 110, 6488-6493, doi:10.1073/pnas.1221312110.
38. Deguine, J.; Bousso, P. Dynamics of NK cell interactions in vivo. Immunol Rev 2013, 251, 154-159, doi:10.1111/imr.12015.
39. Del Monte, U. Does the cell number 10(9) still really fit one gram of tumor tissue? Cell Cycle 2009, 8, 505-506, doi:10.4161/cc.8.3.7608.